Journal of Magnetics 17(1), 1-5 (2012) http://dx.doi.org/10.4283/JMAG.2012.17.1.001

Shape Dependent Coercivity Simulation of a Spherical Barium Ferrite (S-BaFe) Particle with Uniaxial Anisotropy

Gavin S. Abo[1], Yang-Ki Hong[1]*, Jeevan Jalli[1], Jaejin Lee[1], Jihoon Park[1], Seok Bae[1], Seong-Gon Kim[2], Byoung-Chul Choi[3], and Terumitsu Tanaka[4]

[1]*Department of Electrical and Computer Engineering and MINT Center, The University of Alabama, Tuscaloosa, AL 35487, USA*
[2]*Department of Physics and Astronomy, Mississippi State University, Mississippi State, MS 39762, USA*
[3]*Department of Physics and Astronomy, University of Victoria, Victoria, British Columbia, Canada V8W 3P6*
[4]*Department of Information Science and Electrical Engineering, Kyushu University, Fukuoka, Japan*

(Received 9 July 2011, Received in final form 4 February 2012, Accepted 29 February 2012)

The coercivity of a single 27 nm-spherical barium ferrite (S-BaFe) particle was simulated using three models: 1) Gibbs free energy (GFE), 2) Landau-Lifshitz-Gilbert (LLG), and 3) Stoner-Wohlfarth (S-W). Spherically and hexagonally shaped particles were used in the GFE and LLG simulations to investigate coercivity with the different shape anisotropies. The effect of shape was not included in the S-W model. It was found that the models using a spherical shape resulted in a coercivity higher than the models using the hexagonal shape with both shapes having the same diameter. The coercivity estimated with the S-W model was approximately the same as that for the spherical-shape models, which indicates that spherical shape has no significant effect on the particle's coercivity at nanoscale.

Keywords : spherical barium ferrite, micromagnetic simulation, shape anisotropy

1. Introduction

Spherical barium ferrite (S-BaFe: $BaFe_{12}O_{19}$) particles have advantages over metal particles (MP) owing to a point-to-point contact for achieving high areal density for particulate recording media [1-5]. This is mainly because the MP requires a passivation layer that limits reduction of particle size due to low saturation magnetization and coercivity. On the other hand, barium ferrite (BaFe: $BaFe_{12}O_{19}$) particles have the desired properties of high Curie temperature, large saturation magnetization, high coercivity, high magnetic crystalline anisotropy, good chemical stability, and excellent corrosion resistance for magnetic recording media [6]. However, hexagonal platelet barium ferrite (H-BaFe) forms poker-chip-like stacks that limit thorough dispersion of the particles. Although a recording density of 29.5 Gb/in^2 using H-BaFe particles for magnetic tape has been reported [7], further increase of recording density is expected with the development of S-BaFe.

Previous micromagnetic simulations have been performed on single and multiple Fe-Pt and Ni-Fe particles of spherical and hexagonal shapes [8-12], and in particular, on H-BaFe particles [13-16]. It is known that the coercivity of a particle is affected by crystalline anisotropy and shape anisotropy. However, micromagnetic simulation results on a nanosized S-BaFe particle are not yet known to have been reported.

In this paper, the coercivity of a single 27 nm-spherical barium ferrite particle is simulated using three models: 1) Gibbs free energy (GFE) [17], 2) Landau-Lifshitz-Gilbert (LLG) [17], and 3) Stoner-Wohlfarth (S-W) [18]. For the GFE and LLG models, both hexagonally and spherically shaped particles were used to determine the difference in coercivity due to shape anisotropy and to investigate possible microstructures of the S-BaFe particle. This is because the S-BaFe particle may actually be a hexagonal BaFe particle surrounded by Fe_xO_y to give its sphere-like shape, as shown in Fig. 1(a), rather than being entirely spherical. The structure was surmised from TEM micrograh [2] with partial TEM micrograph shown in Fig. 1(b). The S-W model, with excluded shape effect, was used as a reference for the other models.

*Corresponding author: Tel: +1-205-348-7268
Fax: +1-205-348-6959, e-mail: ykhong@eng.ua.edu

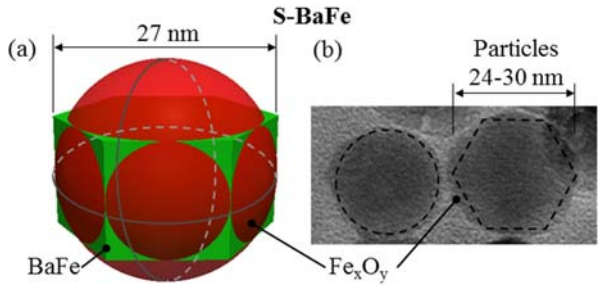

Fig. 1. (a) (Color online) Artist's drawing (rendered in ParaView) of S-BaFe structure as hexagonal BaFe surrounded with Fe_xO_y and (b) partial TEM micrograph from Fig. 5 of [2] with added dotted outline of a hexagon and sphere.

2. Micromagnetic Computer Simulation

The experimentally measured coercivity, saturation magnetization, and remanent magnetic moment of ~27 nm S-BaFe particles are 3211 Oe, 38.7 emu/g, and 22.7 emu/g, respectively [19]. The saturation magnetization, M_s, in emu/cm^3 was estimated using the well-known BaFe theoretical density of 5.29 g/cm^3. The calculated M_s of 204.72 emu/cm^3 (or saturation polarization $J_s = \mu_0 M_s$ in SI units, where μ_0 is the permeability of free space) was used in the simulations. Assumed simulation parameters for BaFe follow. An anisotropy constant K_1 of 3×10^5 erg/cm^3 for S-BaFe was used for all simulations. An applied field 1° from the z-axis in the x-z plane was used to break the symmetry. All simulations are at 0 K.

The GFE and LLG simulations were performed using the magpar simulator [17]. This micromagnetic simulator is based on the finite element method. A unit radius sphere and unit 1 by 0.5 thick hexagonal prism were meshed with a very fine nonuniform tetragonal grid (maximum edge length of tetragonal cell is ~6.5 nm and ~10.8 nm for sphere and hexagon, respectively) with Netgen [20]. The discretized sphere or hexagon were used to define the magnetic region in the simulation. The uniaxial anisotropy direction was set in the z-direction, and the exchange constant was set to 1.3×10^{-6} erg/cm. The maximum edge length is less than the exchange length of ~20.8 nm ($l_{ex} = \sqrt{A/K_1}$ in cgs emu units). The initial magnetization was set in the z-direction (i.e., $M_z = 1$), and the demagnetization field was taken into account for the simulation. The applied field was swept from about 5 kOe (398 kA/m) to –5 kOe in about –5 Oe steps (–0.4 kA/m) to plot half a hysteresis loop. To construct the complete half loop, the condition that stops the simulation when saturation polarization is parallel to the applied external field was disabled (i.e., J//Hext = –1e99). The initial state for the simulation is shown in Fig. 2.

For the Gibbs free energy (GFE) model, the total Gibbs free energy is minimized using magpar by the TAO (Toolkit for Advanced Optimization) module with the limited memory variable metric (LMVM) algorithm. The total Gibbs free energy is the sum of the exchange w_{exch}, anisotropy w_{ani}, Zeeman w_{ext}, and demagnetization w_{demag} energies [17]:

$$\begin{aligned} E_{tot} &= \int_\Omega (w_{exch} + w_{ani} + w_{ext} + w_{demag}) dv \\ &= \int_\Omega (A((\nabla u_x)^2 + (\nabla u_y)^2 + (\nabla u_z)^2) \\ &+ K_1(1 - (\boldsymbol{a} \cdot \boldsymbol{u})^2) - \boldsymbol{J} \cdot \boldsymbol{H}_{ext} - \frac{1}{2} \boldsymbol{J} \cdot \boldsymbol{H}_{demag}) dv \,, \end{aligned} \tag{1}$$

where

$$\boldsymbol{J}(x,t) = J_s(x) \cdot \boldsymbol{u}(x,t), |\boldsymbol{u}| = 1 \tag{2}$$

is the magnetic polarization as a function of space and

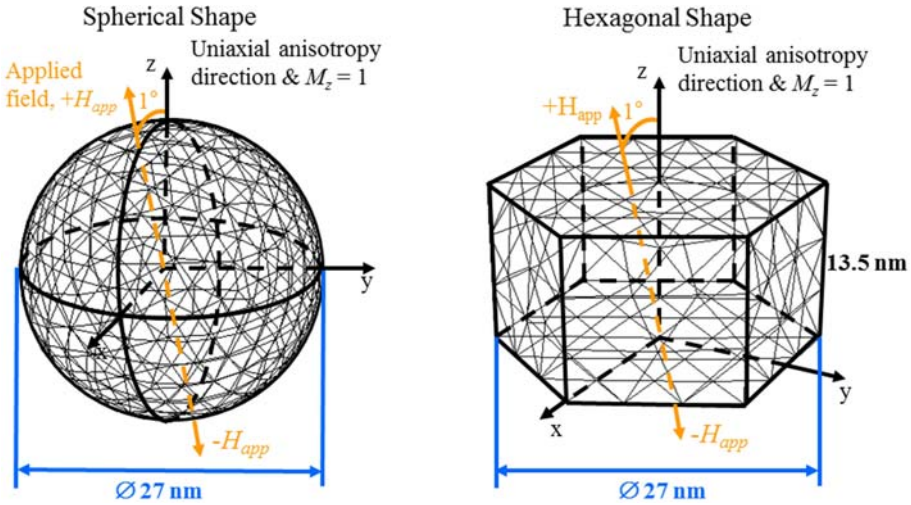

Fig. 2. (Color online) Initial state for the simulation of spherical and hexagonal shape.

time, A is the exchange constant, K_1 is the first magneto-crystalline anisotropy constant, $\boldsymbol{a}$ is the unit vector parallel to the easy axis, $\boldsymbol{H}_{\text{ext}}$ is the external field, and $\boldsymbol{H}_{\text{demag}}$ is the demagnetization field. The u_x, u_y, and u_z are the direction cosines of the magnetization for the position vector $\boldsymbol{u} = u_x\boldsymbol{i} + u_y\boldsymbol{j} + u_z\boldsymbol{k}$.

For the LLG model, the LLG equation is time integrated using magpar by the PETSc (Portable Extensible Toolkit for Scientific computation) module with the backward differentiation formula (BDF). The LLG equation [17] is

$$\frac{d\boldsymbol{J}}{dt} = -\gamma'\boldsymbol{J}\times\boldsymbol{H} - \frac{\alpha\gamma'}{J_s}\boldsymbol{J}\times(\boldsymbol{J}\times\boldsymbol{H}), \quad (3)$$

where $\gamma' = \gamma/(1+\alpha^2)$ and $\boldsymbol{H}$ is the magnetic field, γ is the gyromagnetic ratio, and α is the damping constant. To complete the half loop for the time integration, the maximum simulation time was disabled (i.e., set to 1e99). A Gilbert damping constant, α, of 0.1 was used for all magpar simulations.

For the S-W model, the following equation is solved, such as with C-program language, for the normalized magnetization derived by Usov and Grebenshchikov for the ultimate S-W loop [18].

$$\frac{M_h}{M_s V} = m_h^{SW}(h_e,\theta_0) = \begin{cases} \cos[\theta_0 - \theta_{\min,2}(h_e)], & h_e \geq -h_c \\ \cos[\theta_0 - \theta_{\min,1}(h_e)], & h_e < -h_c \end{cases} \quad (4)$$

where $h_e = H_0/H_k$ is the effective applied field, H_0 is the applied external uniform magnetic field at an angle θ_0 in the x-z plane from the z-axis, $H_k = 2K_1/M_s$ is the crystalline anisotropy field, V is the particle volume, h_c is the critical field, M_h is the magnetization at the given applied field, and the angles of energy minimums are $\theta_{min,1}$ and $\theta_{min,2}$. This equation is applicable to an assembly of oriented particles with uniaxial anisotropy and does not take the shape parameters into account.

3. Results and Discussion

Fig. 3(a) and 3(b) shows the hysteresis loops of a single 27 nm-S-BaFe particle by the three simulations. The experimental loop is also shown of a collection of non-oriented ~27 nm S-BaFe particles heat-treated at 750 °C for 5 h, which was previously reported [19].

Only half hysteresis loops are given in Fig. 3 for the magpar results. The GFE and LLG results of S-BaFe modeled by a 27 nm diameter spherically shaped particle and the ultimate S-W loop overlap in Fig. 3, but have been plotted separately for clarity. The matching coercivity of the S-W loop with the coercivities of the spherical models indicates that the spherical shape has no effect on the particle's coercivity. On the other hand, the S-BaFe particle could possibly be a hexagonal prism, but surrounded by Fe_xO_y to give its spherical shape. This shape may be supported by Mössbauer spectra of S-BaFe nanoparticles with enhanced magnetic properties (coercivity of 4075 Oe, saturation magnetization of 41.4 emu/g, and remanent magnetic moment of 24.3 emu/g) formed by heat-treatment at 900 °C for 2 h that showed the presence of residual hematite (α-Fe_2O_3) phase [2].

The GFE and LLG loop of the S-BaFe modeled by a 27 nm by 13.5 nm thick hexagonal prism shows lower coercivity, H_c, compared to the spherical shape results. The spherically shaped particle shows a H_c closer to the experimental. This suggests that the experimental S-BaFe nanoparticles could more likely be completely converted to near perfect S-BaFe spheres, though there is currently not enough evidence to fully support whether the simulated

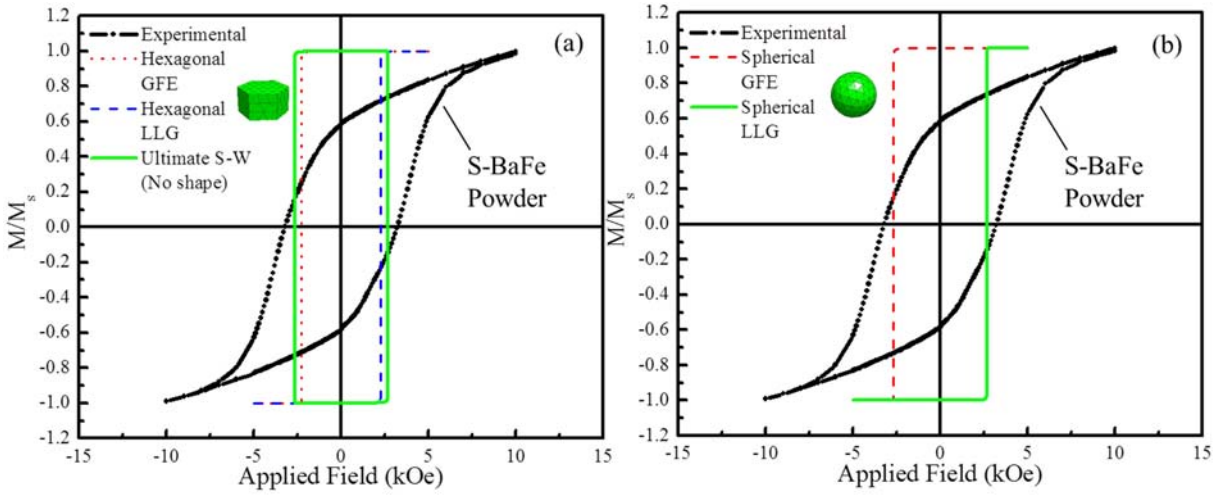

Fig. 3. (Color online) Hysteresis loops of (a) hexagonal GFE, LLG, and S-W and (b) spherical GFE and LLG of 27 nm-S-BaFe particle. Also, experimental loop (non-oriented) previously reported [19].

Table 1. Spherical barium ferrite coercivities simulated by Gibbs free energy (GFE), Landau-Lifshitz-Gilbert (LLG), and Stoner-Wohlfarth (S-W) models and experimentally measured.

Method	Experimental (Non-oriented)	Hexagonal GFE	Hexagonal LLG	Ultimate S-W	Spherical GFE	Spherical LLG
H_c (kOe)	3.2	2.3	2.2	2.7	2.7	2.7

and experimental coercivitities are related and match. Evidence of the near spherical shape is given by the TEM micrographs in [2].

It is noted that the spherical particle was also meshed with a fine nonuniform tetragonal grid with Netgen, then one refinement (for ~7.8 nm maximum edge length) of the mesh was made with magpar. In addition, one refinement by magpar of the hexagonal mesh with very fine nonuniform tetragonal grid (~10.8 nm maximum edge length) to ~8.3 nm maximum edge length was performed. There were almost no changes in results for all magpar simulations with the refined meshes except for the energy minimization simulation on the hexagonal shape. In this case, the coercivity increased to 4.2 kOe.

The coercivities obtained using the three models are summarized in Table 1. All simulated coercivities (at 0 K) are less than the experimental (at room temperature). This is expected since barium ferrite has a positive temperature coefficient, dH_c/dT, such that coercivity (H_c) increases with temperature (T) up to about 423 K [21-24]. Overall, all hysteresis loops show single domain switching that does not correspond with the experimental data. This is because the three models use the condition of single or oriented particles, but the experimental particles are expected to be non-oriented as no mechanism was employed to orient them. It is important to note that S-BaFe has weak interparticle interaction, which may be possible to neglect, according to strong negative peak of ΔM curve [2], but further studies are needed.

The model of simulating magnetic properties of particulate recording media that combines both packing density theory and micromagnetic simulation using the LLG equation is an extended approach. This approach may produce a more accurate hysteresis loop for the non-oriented experimental nanoparticles [25, 26].

For further simulation analysis, simple Stoner-Wohlfarth calculations were made. The Stoner-Wohlfarth nucleation field (H_N) formula [27] in cgs-emu for coherent rotation (i.e., $H_N = H_c$) is

$$H_c = H_k + H_d, \tag{5}$$

where $H_d = -D_{eff} 4\pi M_s$ is the demagnetization or shape anisotropy field and $D_{eff} = 0$ [8] is the effective demagnetization factor for a sphere. When $D_{eff} = 0$, $H_c = H_k = 2.93$ kOe, which is close to our simulated spherical magpar and ultimate S-W results. This seems to further support our simulated results. This is the theoretical maximum coercivity at 0 K as predicted by equation (5). This is closer to, but less than, the coercivity of the reported experimental data; this is expected as mentioned earlier, since the coercivity is expected to increase with temperature due to a positive temperature coefficient. Yet, these calculations assumed oriented particles. On the other hand, it has been given [28] that for randomly oriented identical non-interacting single-domain particles, the coercivity of equation (5) is reduced by a multiple of 0.48 such that $0.48H_c = 1.4$ kOe. Thus, the simulation models may be useful to study partially oriented particles since the simulated coercivities are between the theoretical maximum and randomly oriented coercivity (possibly, the minimum coercivity).

4. Conclusions

The coercivity of a single S-BaFe nanoparticle of 27 nm diameter with uniaxial anisotropy was simulated by three models: 1) Gibbs free energy (GFE), 2) Landau-Lifshitz-Gilbert (LLG), and 3) Stoner-Wohlfarth (S-W). The coherent switching of the simulated hysteresis loops is expected to be due to the single or oriented particle model conditions used for the three models. A model using multiple and randomly oriented particles is expected to be necessary to accurately model the squareness and switching behavior of experimental S-BaFe nanoparticles. The results suggest that the spherical shaped structure is potentially more appropriate for simulating coercivity of S-BaFe nanoparticles. The model using a spherical shape resulted in a coercivity higher than the models using the hexagonal shape with both shapes having the same diameter. Also, the spherical magpar and S-W approach can possibly be used to model the behavior of a single S-BaFe nanoparticle to an oriented assembly.

Acknowledgments

This work was supported by INSIC (Information Storage Industry Consortium) and the E. A. “Larry” Drummond Endowment at the University of Alabama.

References

[1] J. Jalli, Y. K. Hong, J. J. Lee, G. S. Abo, J. H. Park, A. M. Lane, S. G. Kim, and S. C. Erwin, IEEE Magn. Lett. **1**, 4500204 (2010).

[2] J. Jalli, Y. K. Hong, S. Bae, G. S. Abo, J. J. Lee, J. C. Sur, S. H. Gee, S. G. Kim, S. C. Erwin, and A. Moitra, IEEE Trans. Magn. **45**, 3590 (2009).

[3] S. H. Gee, Y. K. Hong, F. J. Jeffers, M. H. Park, J. C. Sur, C. Weatherspoon, and I. T. Nam, IEEE Trans. Magn. **41**, 4353 (2005).

[4] Y. K. Hong, F. J. Jeffers, and M. H. Park, IEEE Trans. Magn. **36**, 3863 (2000).

[5] Y. K. Hong and H. S. Jung, J. Appl. Phys. **85**, 5549 (1999).

[6] H. M. Lee, S. Y. Bae, J. H. Yu, and Y. J. Kim, J. Am. Ceram. Soc. **91**, 2856 (2008).

[7] G. Cherubini, R. D. Cideciyan, L. Dellmann, E. Eleftheriou, W. Haeberle, J. Jelitto, V. Kartik, M. A. Lantz, S. Ölçer, A. Pantazi, H. E. Rothuizen, D. Berman, W. Imaino, P. O. Jubert, G. McClelland, P. V. Koeppe, K. Tsuruta, T. Harasawa, Y. Murata, A. Musha, H. Noguchi, H. Ohtsu, O. Shimizu, and R. Suzuki, IEEE Trans. Magn. **47**, 137 (2011).

[8] T. Schrefl, J. Fidler, and H. Kronmuller, J. Magn. Magn. Mater. **138**, 15 (1994).

[9] W. Scholz, J. Fidler, T. Schrefl, D. Suess, H. Forster, R. Dittrich, and V. Tsiantos, J. Magn. Magn. Mater. **272**, 1524 (2004).

[10] T. Schrefl, G. Hrkac, D. Suess, W. Scholz, and J. Fidler, J. Appl. Phys. **93**, 7041 (2003).

[11] R. P. Boardman, J. Zimmermann, H. Fangohr, A. A. Zhukov, and P. A. J. de Groot, J. Appl. Phys. **97**, 10E305 (2005).

[12] D. R. Fredkin and T. R. Koehler, IEEE Trans. Magn. **25**, 3473 (1989).

[13] R. H. Victora, J. Appl. Phys. **63**, 3423 (1988).

[14] Y. Uesaka, Y. Nakatani, and N. Hayashi, Jpn. J. Appl. Phys. **30**, 2489 (1991).

[15] Y. Nakatani, N. Hayashi, and Y. Uesaka, Jpn. J. Appl. Phys. **30**, 2503 (1991).

[16] Y. Uesaka, Y. Nakatani, and N. Hayashi, Jpn. J. Appl. Phys. **34**, 6056 (1995).

[17] W. Scholz, J. Fidler, T. Schrefl, D. Suess, R. Dittrich, H. Forster, and V. Tsiantos, Comp. Mat. Sci. **28**, 366 (2003).

[18] N. A. Usov and Yu. B. Grebenshchikov, J. Appl. Phys. **106**, 023917 (2009).

[19] J. Jalli, Y. Hong, S. Bae, J. Lee, G. S. Abo, S. Gee, J. C. Sur, and S. G. Kim, Conversion of nano-sized spherical magnetite (S-Mag) to spherical barium ferrite (S-BaFe) nanoparticles for high density particulate recording media, Paper DP-08, presented at Intermag 2009, Sacramento, CA, May 2009.

[20] J. Schoberl, Netgen, http://www.hpfem.jku.at/netgen

[21] O. Kubo and E. Ogawa, J. Magn. Magn. Mater. **134**, 376 (1994).

[22] H. C. Fang, C. K. Ong, X. Y. Zhang, Y. Li, X. Z. Wang, and Z. Yang, J. Magn. Magn. Mater. **191**, 277 (1999).

[23] D. E. Speliotis, IEEE Trans. Magn. **22**, 707 (1986).

[24] J. Wang, F. Zhao, W. Wu, and G. M. Zhao, J. Appl. Phys. **110**, 096107 (2011).

[25] Y. Wang and J. G. Zhu, IEEE Trans. Magn. **45**, 3737 (2009).

[26] B. Biskeborn and P. O. Jubert, IEEE Trans. Magn. **46**, 880 (2010).

[27] R. Skomski, J. P. Liu, and D. J. Sellmyer, J. Appl. Phys. **87**, 6334 (2000).

[28] Z. V. Golubenko, A. S. Kamzin, L. P. Ol'khovik, M. M. Khvorov, Z. I. Sizova, and V. P. Shabatin, Phys. Solid State **44**, 1698 (2002).